# The scintillation mechanisms in Ce and Tb doped $(Gd_xY_{1-x})Al_2Ga_3O_{12}$ quaternary garnet structure crystalline ceramics

M. Korzhik [a,b,*], A. Borisevich [a], A. Fedorov [a,b], E. Gordienko [b,c], P. Karpyuk [b,c], V. Dubov [c], P. Sokolov [b,c], A. Mikhlin [b,c], G. Dosovitskiy [b,c], V. Mechninsky [a,b], D. Kozlov [a], V. Uglov [d]

[a] *Institute for Nuclear Problems of Belarus Stare University, 11 Bobruiskaya, 220030, Minsk, Belarus*
[b] *National Research Center "Kurchatov Institute", Moscow, Russia*
[c] *National Research Center "Kurchatov Institute" – IREA, Moscow, Russia*
[d] *South Ural State University, Chelyabinsk, Russia*

ARTICLE INFO

*Keywords:*
Scintillator
Luminescence
Luminescence kinetics
Scintillation yield
Quaternary compound
Garnet

ABSTRACT

Scintillation mechanisms and performance parameters of quaternary $(Gd,Y)_3Al_2Ga_3O_{12}$ compositionally disordered polycrystalline garnet type ceramics doped with Ce or Tb have been investigated for the first time. Similar light yield dependence on a Gd content in the composition was evidenced for both dopants. The highest light yield achieved in Tb doped samples was found to be four times higher than in Ce doped samples, which was achieved by tuning of the resonance conditions for energy transfer from Gd subsystem to $Tb^{3+}$ activators due to the variation of Gd content in the matrix. The exceptional role of the $Gd^{3+}$ subsystem is forming the high light yield of Tb doped quaternary garnets under different kinds of ionizing radiation is pointed out.

## 1. Introduction

Engineering of compositional disorder in crystalline materials becomes a powerful tool to achieve their new properties [1]. At this view, the modifying of luminescence and scintillation properties of crystalline ternary oxides with garnet structure, activated by $Ce^{3+}$ ions, is the subject of lively discussion in the literature [2]. Variations in a host cationic composition allow controlling both the bandgap and the radiative level position to the bottom of the conduction band, adjusting the luminescence quantum yield [3]. An increase of the cations number in the host compound, that is, the transition from ternary oxides, such as $Gd_3(Ga,Al)_5O_{12}$:Ce to quaternary ones, such as $(Gd,Y)_3(Ga,Al)_5O_{12}$:Ce, increases the compositional disordering. This, was found, leads to further significant improvement in the scintillation parameters: decay kinetics becomes shorter, and a scintillation yield – higher [ 4]. This occurs due to a decrease of a scattering length of nonequilibrium carriers formed by ionizing radiation with the increase of the crystal disorder [5]. At the same time, a compositional disorder in the matrix lattice leads to smearing and modulation of the bottom of the conduction band, which inevitably leads to an appearance of many shallow electron traps, which happen to be the characteristic defects in crystalline ternary oxide compounds already. Their effect on luminescence properties of Ce-activated crystals could be blocked by creating deeper electron traps with a fast recombination time, which is achieved by codoping, e.g., with $Mg^{2+}$ [6] or $Ca^{2+}$ [7] ions, which act as a sink for the electrons from the shallow traps, preventing their release to the conduction band. Codoping at relatively low concentrations do not cause significant deterioration of a scintillation yield [8]. In polycrystalline ceramics, higher $Ce^{3+}$ activator concentrations are achievable compared to melt-grown single crystals, and the effect of shallow traps is neutralized due to the overlap of the Onsager spheres [5] of the $Ce^{3+}$ ions; although an appearance of other types of traps associated with an increased concentration of structural defects near grain boundaries is possible in such materials.

Another activator, not less important for creating bright scintillators is the $Tb^{3+}$ ion. $Gd_2O_2S$ translucent ceramics, activated with $Tb^{3+}$ ions, is widely used in CT scanners [9]. The host compounds for activation with terbium ions, which can be created in a polycrystalline form, are of particular interest [10]. A high concentration of the Tb activator is achievable compared to Ce activator in garnet type crystals [11]. Moreover, high optical transparency is not necessary for the application of a material as a luminescent converter in several applications. This can significantly expand the field of utilization of such scintillation materials, for example, in alpha-voltaics [12], where the efficiency of energy

.

conversion of ionizing radiation can reach or even exceed the efficiency of thermoelectric generators or cathodoluminescent light sources [13]. Moreover, due to high neutron cross-section, cerium doped Gd-based ternary garnets were shown to be promising scintillation materials to detect neutrons in a wide energy range [14,15]. Terbium provides slower but brighter scintillation than cerium, and this makes terbium-activated gadolinium-containing materials promising for application in scintillation threshold neutron counters or neutron sensitive screens, where sensitivity is the most important property.

The aim of this work is to study the effect of the composition of the quaternary oxide compound with a garnet structure $(Gd_xY_{1-x})Al_2Ga_3O_{12}$ (GYAGG) on scintillation properties upon activation with cerium and terbium ions. We have focused on a study of the influence of the Gd to Y ratio variation in the host compound, leaving the Al and Ga ions content constant and close to the ratio, which provides the best scintillation parameters in ternary gadolinium-aluminum-gallium garnet [16]. The studies performed on single-crystal samples doped with cerium ions previously have shown that substitution of Gd by Y up to 20 at.% does not lead to any significant improvement in scintillation properties [17, 18], while a replacement of half of Gd by Y leads to an increase of the yield to the level of 53,000 phot./MeV and make the kinetics close to monoexponential with a decay constant of ~50 ns [4]. The study of the spectroscopic and scintillation properties of crystalline samples of quaternary garnets upon their activation with Tb ions was performed for the first time.

## 2. Samples preparation and measurement procedures

The initial powders series with the $Gd_xY_{2.97-x}Ce_{0.03}Al_2Ga_3O_{12}$ and $Gd_xY_{2.85-x}Tb_{0.15}Al_2Ga_3O_{12}$ compositions were produced using the coprecipitation method. The concentration of Ce was chosen to be ten times high than typical concentration of Ce available in single-crystalline Al–Ga garnets pulled from the melt. Relatively high Ce concentration allowed to diminish the phosphorescence intensity in the crystalline samples, what is typical for Ga–Al mixed crystals. The concentration of Tb was chosen to be close to achieve the highest luminescence yield in the Al-based garnet as described in Ref. [19]. The Gd, Y, Ce, Tb, Al, and Ga mixed nitrate solutions, containing the elements in the ratio according to the formulas, were prepared from Gd, Y and Tb oxides (5 N, 5 N, and 4 N purity respectively), Al hydroxide (5 N) and Ga and Ce nitrates (4 N) and had the concentration of 1 mol/L. Then the solution of each composition was slowly added to the $NH_4HCO_3$ 2 mol/L solution under constant stirring to form a precipitate. The precipitate was filtered, washed with water twice and with isopropyl alcohol once, and calcined at 850 °C for 2 h. Afterward, the powder was milled in a planetary ball mill in corundum grinding media. Green bodies were prepared by uniaxial pressing under 64 MPa. A set of 20 mm tablets was prepared and sintered in air at 1600 °C for 2 h. The resulting ceramics samples were translucent and had a density 98–98.5% of the theoretical value. Samples were polished for the spectroscopic and spectrometric investigation to a thickness of 1 mm. Thus, two ceramics samples series – Ce-doped and Tb-doped, Gd content varying within each series – were prepared.

Scanning electron microscopy (SEM) was performed using Jeol JSM 7100 F in secondary electrons mode at 6 kV. Samples were mirror-polished and thermally etched at 1250 °C for the observation. SEM images of $Gd_{0.89}Y_{2.08}Ce_{0.03}Al_2Ga_3O_{12}$ and $Gd_{0.83}Y_{2.02}Tb_{0.15}Al_2Ga_3O_{12}$ ceramics are shown in Fig. 1. Grains have close sizes in both ceramics: 3–6 μm for the Ce-doped sample and 3–7 μm for the Tb-doped sample.

Photo-excited kinetics of the luminescence of Ce doped samples was measured with Picoquant Fluorotime 250 spectrofluorimeter with LED excitation at room temperature, whereas scintillation kinetics were evaluated from the data obtained by start-stop technique based on measurement of annihilation 511 keV γ-quanta of 22-Na source. Luminescence spectra were measured from the surface of the samples both with spectrofluorometer and SDL-2 luminescence spectrometer.

Ce and Tb doped samples have quite different scintillation kinetics: decay time constants are at the order of a few tens of nanoseconds for $Ce^{3+}$-doped samples, whereas there are of the order of milliseconds for $Tb^{3+}$-doped samples. Therefore, the combined method to evaluate light yield (LY) of the samples under different kinds of ionizing radiation has been applied.

First, γ/α response ratio, characterizing a difference of light yields under γ-quanta and α-particles, was evaluated for different crystals, close to the host compounds under study. Three garnet single crystalline samples, namely $Y_3Al_5O_{12}$:Ce (YAG), $Gd_{1.5}Y_{1.5}Al_2Ga_3O_{12}$:Ce (GYAGG:Ce) and $Gd_3Al_2Ga_3O_{12}$:Ce (GAGG:Ce), which are available at the market, having typical Ce concentration at the level of 800–900 ppm, 1 mm thick, were used for γ/ α response ratio measurements through the standard procedure of pulse height spectra acquisition under $^{137}Cs$ ($E_\gamma$ = 662 keV) and α-particles of $^{241}Am$ ($E_\alpha$ = 5 MeV) using Hamamatsu R329 photomultiplier at room temperature. CsI(Tl) reference crystal with light yield 54,000 ph/MeV under γ-excitation was used as a reference. Error of light yield measurements was estimated to be ± 1%. One ceramic sample (Gd content x =1.49) was cut and polished to 0.3 mm thickness in order to make it semitransparent and used for similar measurements. A decrease of the γ/ α response ratio in the ceramic sample, having one order of magnitude higher concentration of activator compared to the single crystals, is in good agreement with the same behavior demonstrated for YAG:Ce ceramics [20]. Table 1 summarizes the measurement results of the γ/α and light yield for the materials of choice.

The relative light yield of Ce-doped ceramic samples was measured using a reference YAG:Ce single crystal with Philips XP2020 PMT in a pulse height and current modes. The samples were mounted at 45° angle to the PMT photocathode window as described in Ref. [21], and were

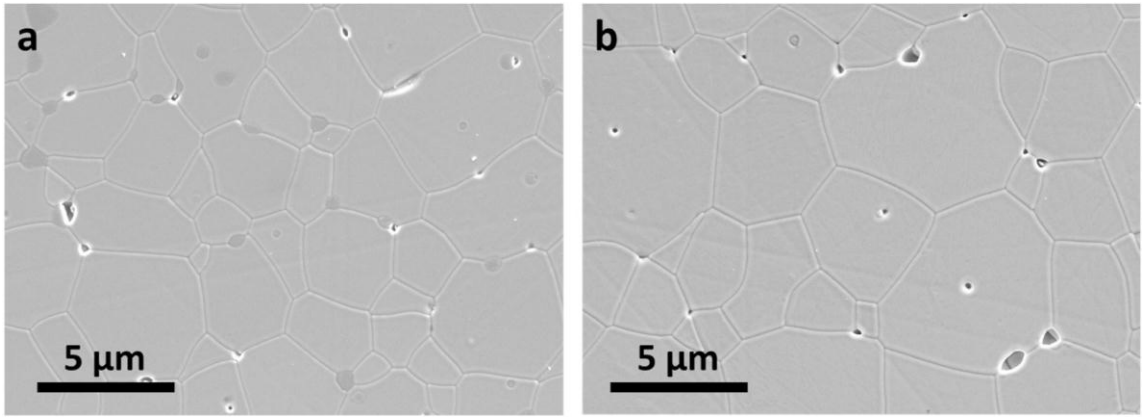


**Fig. 1.** SEM images of $Gd_{0.89}Y_{2.08}Ce_{0.03}Al_2Ga_3O_{12}$ (a) and $Gd_{0.83}Y_{2.02}Tb_{0.15}Al_2Ga_3O_{12}$ (b) ceramics samples.

**Table 1**

Light yield under γ- and α-excitation and γ/α response ratio of YAG, GYAGG, GAGG garnet type scintillators doped with Ce.

| Material | YAG, single crystal | GYAGG: Ce, single crystal | GAGG: Ce, single crystal | GYAGG:Ce, ceramics |
|---|---|---|---|---|
| Light yield, ph/MeV under Eγ =662 keV | 20,600 | 47,600 | 36,000 | 38,900 |
| Light yield, ph/MeV under Eα =5 MeV | 3890 | 11,670 | 7060 | 13,400 |
| γ/α response ratio | 5.32 | 4.77 | 5.1 | 2.8 |

excited by the α-particles of $^{241}$Am source and the total activity of $10^4$ Bq. A diaphragm with a diameter of 6 mm was placed between the source and the measured sample to ensure the number of alpha-particles reaching the face surface of all samples is equal. PMT anode current was integrated over time with a time constant of 0.1 s and its value was measured with a digital multimeter. Error of measurements was estimated to be±2%. The light yield of each sample was supposed to be proportional to the PMT anode current measured with the alpha-source excitation after subtraction of the PMT "dark" current, measured without the alpha-source. The pulse height spectra measurements were performed to obtain maxima of the total absorption peaks of α-particles with a standard pulse height technique for Ce-doped samples only. The measurement procedure in a current mode was applied to Tb-doped samples.

## 3. Results

Fig. 2 shows the light yield values of the $Gd_xY_{2.97-x}Ce_{0.03}Al_2Ga_3O_{12}$ ceramics samples with different Gd content ($x$) in the composition measured under excitation with α-particles in the pulse height mode and the light yield of the same samples under γ-quanta, calculated through γ/α response ratio for ceramics. The light yield values of the reference Ce-doped GAGG and GYAGG single crystal samples measured under α-particles and γ-quanta (662 keV, directly measured) are also included for comparison. Single crystals demonstrate rather higher light yield under γ-quanta, which corresponds to their higher γ/α ratio.

Fig. 3 shows the deconvolution results of photoluminescence kinetics at excitation 340 nm in the $5d_2$ level of $Ce^{3+}$ ion and of scintillation kinetics at room temperature for Ce-doped samples. Photoluminescence kinetics is approximated with three components rather well, whereas scintillation kinetics – with two exponents only. Photoluminescence kinetics decay constants depend on the Gd content in the material: all samples demonstrate two fast and one slow components, which tend to diminish at x ⩾1.2. Note, GYAGG single crystal having composition Gd/Y =1 and roughly ten times less Ce concentration has photoluminescence decay constant 55 ns?as described in Ref. [4]. Meanwhile, Fig. 4 shows a change of the peak and integral intensity of the luminescence at the intracenter excitation in the peak maximum of the $^2F_{5/2} \rightarrow 5d_1$ transition. Both results suggest a combined mechanism of the luminescence quenching: concentration quenching due to a large Ce concentration and, additional quenching of $Ce^{3+}$ ions by $Gd^{3+}$ subsystem.

Scintillation kinetics decay constants were found to be weakly depending on Gd content as well; two components were distinguished – ~28 ns (fast) and ~140 ns (slow) for all Ce-doped samples. However, their fractions changed substantially: the fraction of the fast component decreased with the Gd content increase, and vise versa for the slow component.

Fig. 5 shows the light yield (relatively to YAG:Ce) of the Ce-doped ceramic samples measured with Philips XP2020 PMT in pulse height and current modes and R329 PMT in pulse height mode, for different Gd contents in the composition. The results, given by both methods for light yield estimation, correlate quite well.

The light yield of $Gd_xY_{2.85-x}Tb_{0.15}Al_2Ga_3O_{12}$ ceramics series was evaluated relatively to YAG:Ce in the current mode with the same bench using XP2020 PMT. The measurement results are given in Fig. 6 along with the light yield of a GAGG:Tb single crystalline sample, doped with the same amount of Tb as ceramics and measured in the same conditions. Assuming that response ratio γ/α= 2.8 is valid for the scintillator doped with Tb, we have estimated response of the Tb doped ceramics to γ-quanta. These results are also plotted in Fig. 6.

One can state, that both Ce- and Tb- doped ceramics show similar light yield behavior with the change of the Gd content in the composition, which is observed in mixed crystals quite often [22]. However, Tb doped samples demonstrate extremely high light yield both under α- and γ-excitation indicating an exceptionally efficient mechanism of transformation of nonequilibrium carriers energy into an ensemble of excited $Tb^{3+}$ ions.

The phase composition of the samples was studied by XRD using

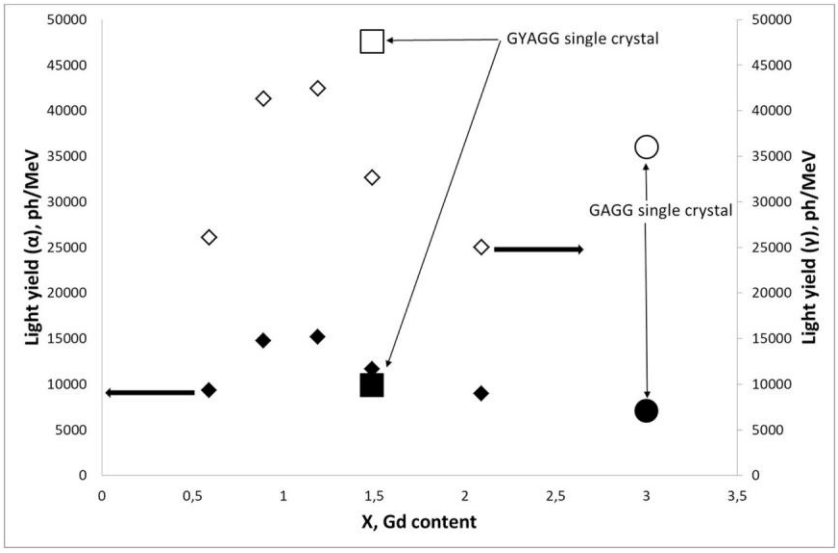


**Fig. 2.**Light yield of the ceramics samples $Gd_xY_{2.97-x}Ce_{0.03}Al_2Ga_3O_{12}$ measured under $^{241}$Am α-particles excitation (filled diamonds) and calculated through γ/α response for γ-quanta excitation (hollow diamonds) for different Gd content $x$ in the composition. Measured light yield of the reference GAGG:Ce, Mg and GYAGG:Ce, Mg single crystalline samples under 662 keV γ-quanta (hollow symbols) and calculated response to α-particles (filled symbols).

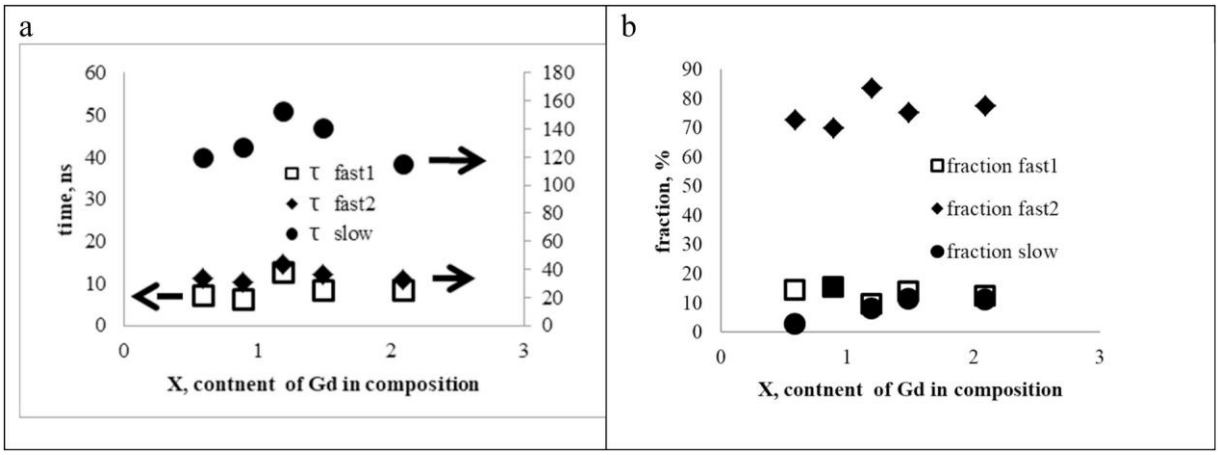


**Fig. 3.**Parameters of the deconvolution of the kinetics decay curves for photoluminescence (excited at 340 nm) (a,b) and scintillation (c,d) of Gd $_x$Y$_{2.97-x}$Ce$_{0.03}$Al$_2$Ga$_3$O$_{12}$ samples with different Gd content (x) in the composition. (a, c) – decay constants, (b, d) – fractions of the fast and slow components in the kinetics. Errors: decay constants - ±2%, fractions- ±3%.

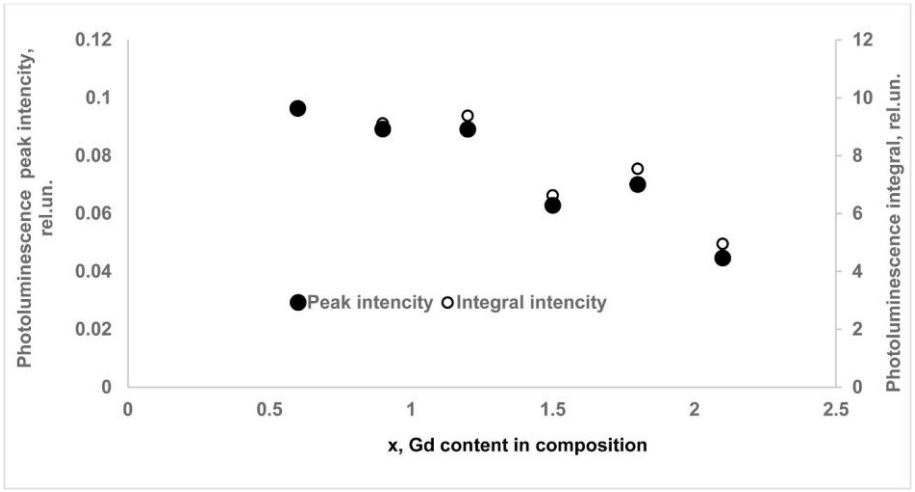


**Fig. 4.**Peak and integral intensity of the photoluminescence Gd $_x$Y$_{2.97-x}$Ce$_{0.03}$Al$_2$Ga$_3$O$_{12}$ samples with different Gd content (x) in the composition.

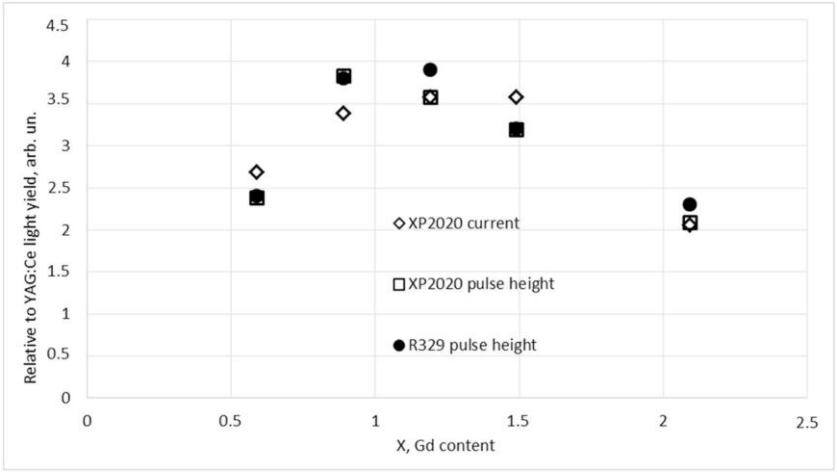


**Fig. 5.**Relative to YAG light yield of the ceramics samples Gd $_x$Y$_{2.97-x}$Ce$_{0.03}$Al$_2$Ga$_3$O$_{12}$ under excitation with α-particles of $^{241}$Am at different Gd content *x* in the composition measured with R329 PMT in pulse height mode and XP2020 PMT in pulse height and current modes.

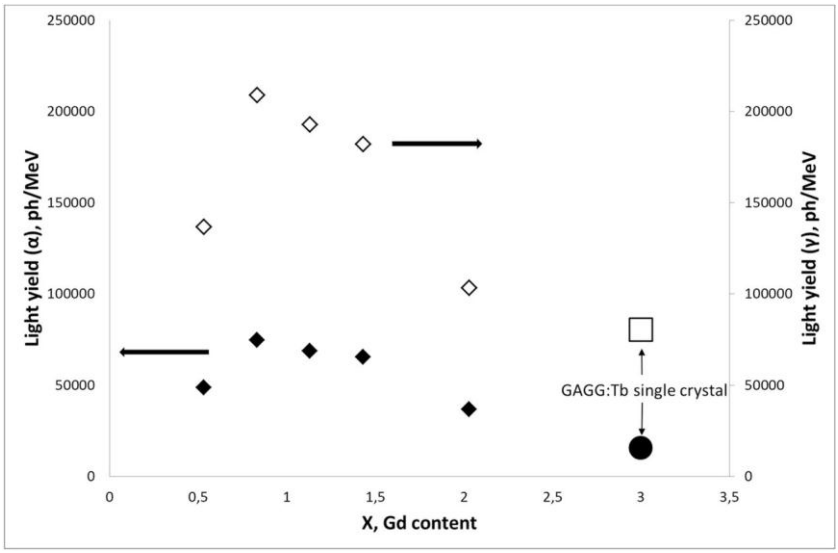


**Fig. 6.** Measured light yield of the ceramics samples $Gd_xY_{2.85-x}Tb_{0.15}Al_2Ga_3O_{12}$ under excitation with α-particles of $^{241}Am$ (filled diamonds) and calculated through γ/α = 2.8 the light yield of the samples under γ-quanta (hollow diamonds) at different Gd content (*x*) in composition, and of the reference GAGG:Tb single crystal.

Rigaku ULTIMA IV diffractometer in the parallel beam geometry using $Cu_{K\alpha}$ radiation with a wavelength of 0.154179 nm in the angle range 2θ = 10–120 °, with a step of 0.05° and the detector movement speed 2°/min. The phase composition was determined using the PDXL-2 software (Rigaku); a single garnet phase was found for all the samples. The average error in lattice parameter determination is 0.02%. Fig. 7 shows the change of the lattice parameter of ceramic samples versus Gd content in the composition.

The lattice parameters values for the $Gd_xY_{2.85-x}Tb_{0.15}Al_2Ga_3O_{12}$ series is consistent with the known values for the ternary garnets however, the dependence on Gd content was found to differ from linear: it seems to consist of 2 parts for samples having smaller and larger Gd content relative to the composition with equal Gd and Y content. It is interesting to note, the change of the lattice parameter dependence motive in the middle point correlates with the break in the LY dependence on Gd content both for Ce and Tb doped samples. An increase is substituted with a decrease of the LY, and slower kinetics occur.

The room temperature photoluminescence spectrum for the $Gd_{0.53}Y_{2.32}Tb_{0.15}Al_2Ga_3O_{12}$ sample and luminescence excitation spectra of the Tb doped series of the samples is given in Fig. 8. The photoluminescence spectrum is typical for $Tb^{3+}$ in many luminescent materials [25] and contains bands, which correspond to *f-f* electronic transitions from $^5D_{3,4}$ levels to components of $^7F_j$ term. The excitation spectra contain *f-f* excitation bands, as well as *f-d* bands [26] with maxima below 330 nm. The excitation spectra are normalized to the maximum of the group of f-d bands in the 250–290 nm region; one could see, that both groups of *f-d* bands experience small peak position variations with a change of the Gd content in the ceramics.

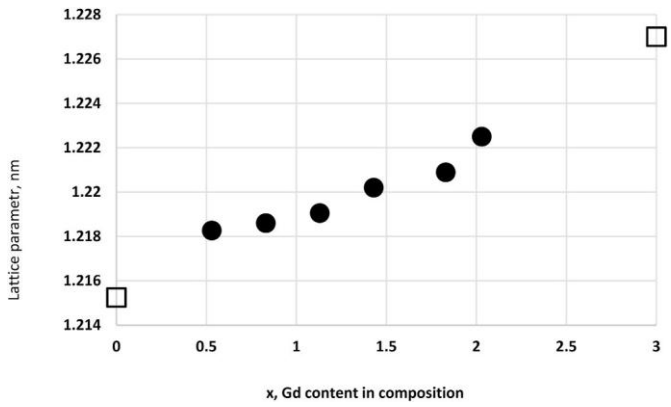


**Fig. 7.** Lattice parameter of $Gd_xY_{2.85-x}Tb_{0.15}Al_2Ga_3O_{12}$ at different Gd contnent x in the ceramics composition. Hollow spots are lattice parameters of $Y_3Ga_3Al_2O_{12}$ [23] and $Gd_3Ga_3Al_2O_{12}$ [24].

## 4. Discussion

Our results show that both Ce and Tb doped quaternary garnets show similar light yield dependence on the Gd content. It can be explained by the change of the role of Gd sublattice in the energy transfer processes in the garnet crystal lattice. Gd and Y ions occupy the same type of lattice sites – dodecahedral – in the garnet crystal lattice. Table 2 shows the average distance $R_{hd}$ between $Gd^{3+}$ ions in the $Gd_xY_{3-x}Al_2Ga_3O_{12}$ host, estimated in an approximation of homogeneous dilution. Gd ion site in GAGG has four $Gd^{3+}$neighbors at the distance of 3.754 Å and next four neighbors at the distance of 5.735 Å [27]. The distances at x < 3 were evaluated for the lattice parameters shown in Fig. 7. For Gd index x = 3 in $Gd_xY_{3-x}Al_2Ga_3O_{12}$ (100% occupancy), the average distance to the nearest Gd neighbor is 3.754 Å. As Gd content decreases, the average distance increases proportionally to the reverse cube root of the volume concentration (e.g. for Gd index 0.375, site occupancy is 1/8 and the average Gd–Gd distance doubles). The right column in the table shows $(R_{hd}(x = 3)/R_{hd}(x))^6$, which illustrates a change of the energy transfer probability from the Gd subsystem to activator ions on concentration. Apparently, a strong influence of the Gd concentration index on the donor ($Gd^{3+}$)→acceptor (activator) transfer rate $K_{da}(r) = \tau_d^{-1}(R_{da}/r)^6$, where $\tau_d$ is donor radiating time and $R_{da}$-constant, characterising Coulomb donor-acceptor interaction, is compensated by the two opposite processes: (1) reducing of a migration quenching with the dilution of the Gd sub-system and (2) increase of the role of the excitation transfer from autholocalised excitonic states, which are distinctive for Y based garnets [5]. The combination of these processes forms the LY dependence at $x < 1.5$. As seen from Fig. 7, discontinuity in curve smoothness of the lattice parameter was observed in the vicinity of $x \approx 1.4$. Light yield dependencies have their maxima near Gd index $x = 1.2$. This is close to the site percolation threshold for the lattice having four similar cations in the first coordination sphere – 0.43 [28], which corresponds to x = 1.3. At high indexes, the same ion can always be found in the first cation coordination sphere, which promotes a formation of continuous subbands for migration of Frenkel excitons inside the forbidden zone.

The LY (Fig. 2) and photoluminescence integral intensity (Fig. 4)

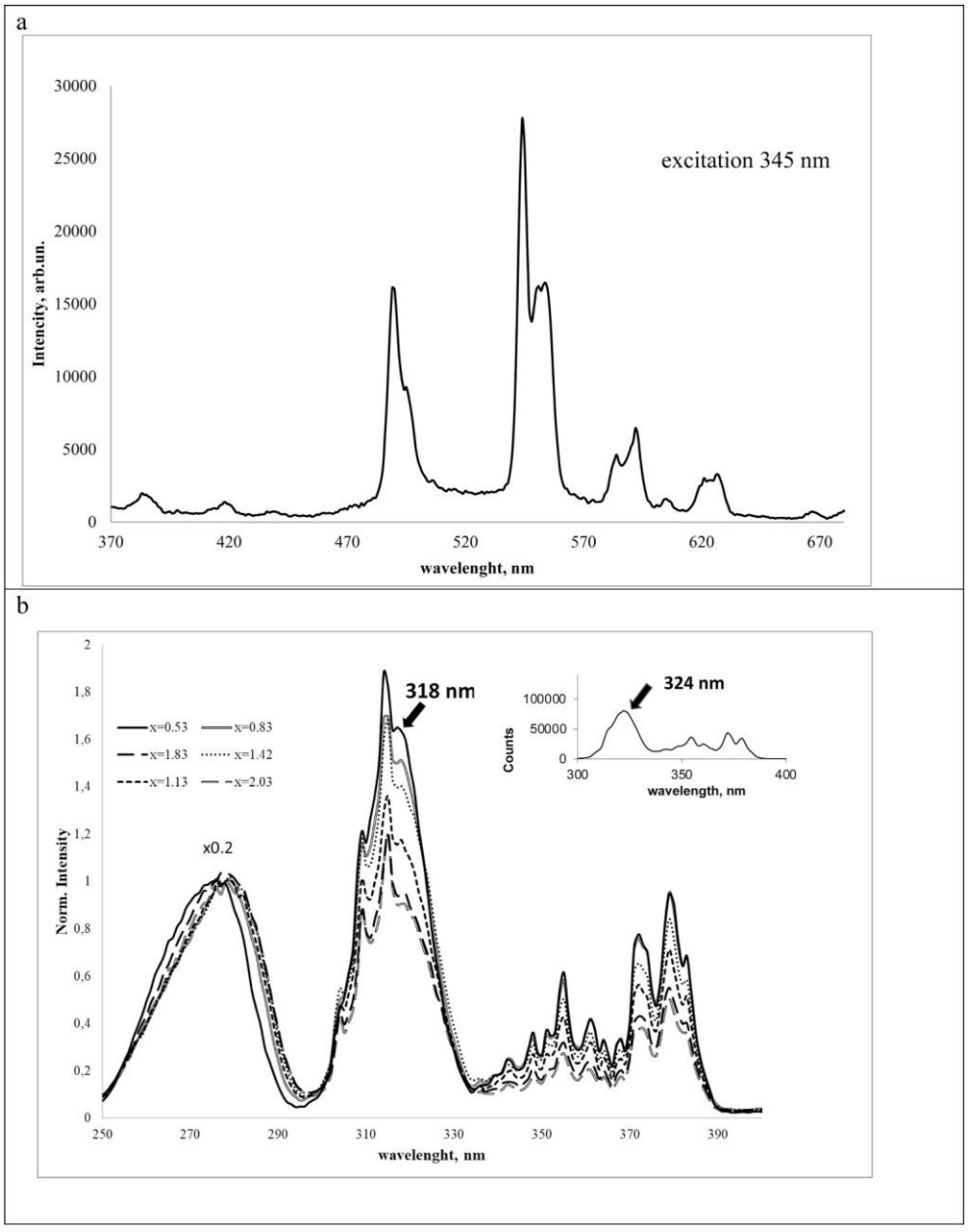


**Fig. 8.**Photoluminescence spectrum of sample $Gd_xY_{2.85-x}Tb_{0.15}Al_2Ga_3O_{12}$ for x =0.53 under excitation at 345 nm (a), luminescence excitation spectra for the whole series, registration wavelength – 545 nm, the spectra are normalized to 278 nm peak intensity (b), and single crystal $Gd_{2.85}Tb_{0.15}Al_2Ga_3O_{12}$ luminescence excitation spectrum (inset).

**Table 2**
Average distance $R_{hd}$ between $Gd^{3+}$ ions in the $Gd_xY_{3-x}Al_2Ga_3O_{12}$ host for different Gd indexes.

| Gd index | Y index | $R_{rm}$, Å | $(R_{hd}\ (x=3)/R_{hd}(x))^6$ |
|---|---|---|---|
| 3 | 0 | 3.754 | 1 |
| 2.1 | 0.9 | 4.228 | 0.49 |
| 1.8 | 1.2 | 4.451 | 0.36 |
| 1.5 | 1.5 | 4.730 | 0.25 |
| 1.2 | 1.8 | 5.095 | 0.16 |
| 0.9 | 2.1 | 5.608 | 0.09 |
| 0.6 | 2.4 | 6.419 | 0.04 |
| 0.375 | 2.625 | 7.508 | 0.015 |

reduction, which is observed with further increase of Gd concentration in the crystal at x >1.2, could be explained by an increase of a migration quenching [29] in the Gd subsystem because of faster diffusion of Frenkel type excitons along the subzones created by $^8S$, $^6P$ states. Really, the diffusion probability in the donor system is $\sim C^1_D/_D{}^2$ when it occurs due to jumps between relatively sparsely placed ions, whereas it is $\sim C^3_D/_D{}^4$ in the case of diffusion in the sublattice of the equivalent ions.

The said above explains the LY behavior versus the Gd content qualitatively, but it does not explain the large difference in the LY of the Ce and Tb doped garnets. In order to clarify the origin of the high LY of the Tb doped samples, we have built an electronic energy levels diagram of the major ions acting in the energy transfer: $Ce^{3+}$, $Gd^{3+}$ and $Tb^{3+}$. Fig. 9 illustrates the disposition of the electronic energy levels in $Gd_{1.48}Y_{1.48}Ce_{0.03}Al_2Ga_3O_{12}$ and $Gd_{1.42}Y_{1.42}Tb_{0.15}Al_2Ga_3O_{12}$ crystalline compounds. The bandgap $E_g$ for both compounds was chosen to be 6.4 eV.

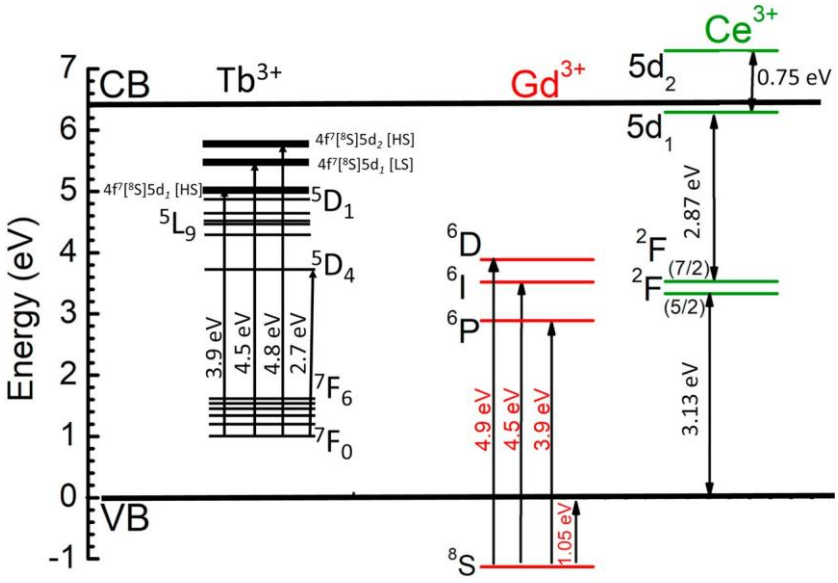


**Fig. 9.**Scheme of the electronic energy levels in $Gd_{1.48}Y_{1.48}Ce_{0.03}Al_2Ga_3O_{12}$ and $Gd_{1.42}Y_{1.42}Tb_{0.15}Al_2Ga_3O_{12}$.

It is known that the excitonic excitation transfer mechanism dominates in garnet type $Ce^{3+}$ doped materials while scintillation occurs [5]. Contrary to the crystals on a base of Y, La, Lu, which have no peculiarities of the electron density states peculiarities into the forbidden zone, the Gd3 +based crystal host has numerous *f*-levels ( $^6$P, $^6$I, $^6$D) creating sub-zones in the bandgap. Moreover, following to extended Dieke diagram [30], one can suppose that numerous $Gd^{3+}$ levels in the energy ranger above 40000 $cm^{-1}$ will provide a chain of consecutive processes which include effective capture of nonequilibrium carriers by Gd ions and intracenter relaxation to $^6P$ state. The intracenter relaxation process is quite short and carries on within a few ps [31]. So, besides the lattice excitons having energy slightly less than bandgap energy, the significant part of nonequilibrium carriers create Frenkel type excitons, which have a capability for migration along with $^6P$, $^8S$ states of $Gd^{3+}$ sublattice. For these excitons, the energy required to create one pair of nonequilibrium carriers is less by number 6.4(*Eg*)/3.9 ($^8S$–$^6P$ transition energy) =1.6 than for regular autholocalized excitons. Due to this reason, Tb doped scintillator materials have a potential for better LY in a comparison with Ce doped species.

The Gd sub-system does contribute to populating the $Ce^{3+}$ radiating level through an interaction of the Frenkel exciton and $^2F_{5/2} \rightarrow 5d_2$ transition however, resonance actually is poor, and involvement of the phonons is required. Moreover, $5d_2$ level is located in a conduction band, so a delocalization of electrons occurs allowing nonradiative recombination of nonequilibrium carriers.

Meanwhile, holes can be quickly delocalized to the top of a valence band from $^8$S state [8]. Spatially, the hole can be localized in the same polyhedron with the mother Gd ion, but predominantly located at the coordinating oxygen. The following transfer process, which is caused by the resonance between $^2F_{5/2} \rightarrow 5d_1$ and $^6P \rightarrow VB_{top}$ (top of the valence band), can contribute to the LY increase of quaternary Gd-based garnets as well. Apparently, such an assignment of holes to those localized on the cation and anion is rather arbitrary at a relatively high measurement temperature; localization occurs rather on hybridized orbitals, and the Frenkel exciton should be considered as localized on the oxy-anionic complex.

**Table 3**
Some parameters of the electronic energy levels disposition in YAG, GYAGG (Gd/Y =1), and GAGG doped with Ce and Tb. E1 – energy difference between $^2F_{5/2}$ and top of the valence band, E2 – energy difference between $5d_1$ state and bottom of the conduction band, E3 – energy difference between $^7F_0$ and $4f^7$ [$^8S$] $5d_1$ [HS] levels.

| Crystal | YAG [26] | YAGG [2] | GYAGG | GAGG |
|---|---|---|---|---|
| E1 (Ce doping), eV | 3.05 | 3.12 | 3.13 | 3.35 |
| E2 (Ce doping), eV | 1.2 | 0.43 | 0.4 | 0.3 |
| E3 (Tb doping), eV | 3.86 | | 3.92 | 3.85 |

Table 3 summarizes some parameters of the $Ce^{3+}$ and $Tb^{3+}$ energy levels disposition in binary, ternary, and quaternary garnets. The position of $Ce^{3+2}$ *F* levels shows a minor energy increase in the hosts from YAG to GAGG, whereas the position of $5d_1$ level relative to the conduction band bottom is controlled by a crystal field strength: the smaller the cation substituted by $Ce^{3+}$ ion is, the larger shift occurs. The effect of the crystal field moves $5d_2$ component down as well: the energy of the transition from the ground state decreases with the amount of Y in the matrix. This leads to an increase in the detuning of the Frenkel exciton from $Ce^{3+}$ transitions and contributes to a decrease in the scintillation yield with an increase in the fraction of yttrium in the composition. Thus, we conclude, that besides *Al/Ga* ratio in ternary and quaternary garnets, the *Gd/Y* ratio is an effective mechanism for tuning the lower *5d* levels position within the forbidden zone as well as an energy of the first allowed *f-d* transition.

The result of such regulation could be clearly observed in the series of the garnets doped with terbium as well. Terbium luminesce excitation spectra (Fig. 8) show perfect overlapping of $^8S \rightarrow ^6P$ ($Gd^{3+}$) and $^7F_0 \rightarrow 4f^7$ [$^8S$]$5d_1$ [HS] ($Tb^{3+}$) levels. Moreover, the energy of interconfigurational transition can be fine-tuned to obtain the best conditions for dipole-dipole interaction, as seen from Table 3 (bottom raw). The inset in Fig. 8(b) demonstrates a weak overlapping of the transitions in Tb-doped ternary GAGG, making its LY at gamma-excitation less than 100,000 ph/MeV. The situation is changed in Y–Gd samples – the energy of the transition $^7F_0 \rightarrow 4f^7$ [$^8S$]$5d_1$ [HS] increases, making perfect conditions for the resonance of this transition with $^8S \rightarrow ^6P$ ($Gd^{3+}$).

At the resonant conditions, the transfer from Frenkel type excitons forms the significant mechanism to populate $Tb^{3+}$ radiation state. In case of the absence of the resonance conditions of energy levels of doping ions and Frenkel type excitons, the latter just recombine non-radiatively. An example is GSO:Ce, where no resonance conditions are and, as consequence, LY is ~10,000 ph/MeV only [22]. Similarly, to the case of Ce ions, the resonance transfer between $^7F_0 \rightarrow ^5D_4$ ($Tb^{3+}$) and $^6P$ ($Gd^{3+}$)$\rightarrow VB_{top}$ can contribute as well. A comparison of the results of LY at gamma-excitation (Figs. 2 and 6) shows that LY in Tb-doped samples is at least 4 times larger than in Ce-doped samples, what rather good correlates with the five-time difference in the activator concentrations.

It could be explained by more efficient competition to quenching centers to catch electronic excitations and additional mechanisms of energy exchange. The dipole-dipole interaction is not the only type of short-range energy transfer. Another type of transfer is the Dexter exchange transfer. Its efficiency falls exponentially with an increase of the distance between donor and acceptor, since this mechanism requires overlapping of wavefunctions of interacting donor and acceptor, and tails of localized wavefunctions fall exponentially with distance. Highly doped with Tb samples meet these requirements making this mechanism to be accountable for the LY increase. Even in GAGG:Tb single crystal, where the detuning of energies corresponding to $^8S\rightarrow{}^6P$ and $^7F_0\rightarrow{}^5D_4$ ($Tb^{3+}$) and $^7F_0\rightarrow{}^4f^7$ [$^8S$]$5d_1$ [HS] transitions is maximal, but $^7F_0\rightarrow{}^5D_4$ ($Tb^{3+}$) and $^4f^7$ $(Gd^{3+})\rightarrow VB_{top}$ resonance still remains, the LY is 80,000 ph/MeV. This is by a factor of ~1.5 higher than the LY of the best GAGG:Ce single crystals, for which the resonance transfer preferably works. Thus, a combination of high Tb concentration and fine-tuning of the resonance conditions in quaternary garnets could benefit in the further gain of the scintillation light yield.

## 5. Conclusions

Two series of scintillation ceramics $Gd_xY_{2.97-x}Ce_{0.03}Al_2Ga_3O_{12}$ and $Gd_xY_{2.85-x}Tb_{0.15}Al_2Ga_3O_{12}$ at different Gd content in the composition were studied. Both compounds demonstrate similar dependence of the light yield on the composition. The maximal luminosity was obtained at the Gd index x = 1–1.2 both for Ce and Tb-doped samples. The observed effect is explained by a change of the conditions for migration of Frenkel type excitons associated with oxy-anionic complexes on a base of $Gd^{3+}$ ions. Changing of the *Gd/Y* ratio in quaternary garnets was found to be an effective mechanism for tuning the lower *5d* levels position within the forbidden zone as well as an energy of the first allowed *f-d* transition for better energy transfer from $Gd^{3+}$ subsystem to activating ions.

## Author statement

It is my pleasure to submit additionally revised manuscript of the article "The scintillation mechanisms in Ce and Tb doped $(Gd_xY_{1-x})Al_2Ga_3O_{12}$ quaternary garnet structure crystalline ceramics" by M. Korzhik, A. Borisevich, A. Fedorov, E. Gordienko, P. Karpyuk, V. Dubov, P. Sokolov, A. Mikhlin, G. Dosovitskiy, V. Mechninsky, D. Kozlov, V. Uglov.

## Declaration of competing interest

The authors declare that they have no known competing financial interests or personal relationships that could have appeared to influence the work reported in this paper.

## Acknowledgements

This work was supported by the grant of Russian Federation Government number 14. W03.31.0004. Experimental equipment was partially provided by NRC "Kurchatov Institute" – IREA shared analytical facilities.

## References

[1] A. Samoilov, A. Goodwin, Designing disorder into crystalline materials, Nat Rev, Chem (2020), https://doi.org/10.1038/s41570-020-00228-3.
[2] J. Ueda, S. Tanabe, Review of luminescent properties of $Ce^{3+}$-doped garnet phosphors: new insight into the effect of crystal and electronic structure, Opt. Mater. X. 1 (2019) 100018–100037.
[3] K. Asami, J. Ueda, M. Kitaura, S. Tanabe, Investigation of luminescence quenching and persistent luminescence in $Ce^{3+}$ doped $(Gd,Y)_3(Al,Ga)_5O_{12}$ garnet using vacuum referred binding energy diagram, J. Lumin. 198 (2018) 418–426.
[4] M. Korzhik, V. Alenkov, O. Buzanov, G. Dosovitskiy, A. Fedorov, D. Kozlov, V. Mechinsky, S. Nargelas, G. Tamulaitis, A. Vaitkevičius, Engineering of a new single-crystal multi-ionic fast and high-light-yield scintillation material $(Gd_{0.5}–Y_{0.5})_3Al_2Ga_3O_{12}$:Ce,Mg, CrystEngComm 22 (2020) 2502–2506.
[5] M. Korzhik, G. Tamulaitis, A.N. Vasil'ev, Physics of Fast Processes in Scintillators, Springer International Publishing, 2020, p. 250.
[6] G. Tamulaitis, A. Vasil'ev, M. Korzhik, A. Mazzi, A. Gola, S. Nargelas, A. Vaitkevičius, A. Fedorov, D. Kozlov, Improvement of the time resolution of radiation detectors based on $Gd_3Al_2Ga_3O_{12}$ scintillators with SiPM readout, IEEE Trans. Nucl. Sci. 66 (2019) 1879–1888.
[7] G. Tamulaitis, E. Auffray, A. Gola, M. Korzhik, A. Mazzi, V. Mechinski, S. Nargelas, Y. Talochka, A. Vaitkevičius, A. Vasil'ev, Improvement of the timing properties of Ce-doped oxyorthosilicate LYSO scintillating crystals, J. Phys. Chem. Solid. 139 (2020) 109356–109367.
[8] E. Auffray, R. Augulis, A. Fedorov, G. Dosovitskiy, L. Grigorjeva, V. Gulbinas, M. Koschan, M. Lucchini, C. Melcher, S. Nargelas, G. Tamulaitis, A. Vaitkevicius, A. Zolotarjovs, M. Korzhik, Excitation transfer engineering in Ce-doped oxide crystalline scintillators by codoping with alkali-earth ions, Phys. Status Solidi 215 (2018) 1700798–1700808.
[9] L. Brixner, New X-ray phosphors, Mater. Chem. Phys. 16 (1987) 253–281.
[10] R. Naik, S. Prashantha, H. Nagabhushana, Y. Naik, K. Girish, Green light emitting $Tb^{3+}$ doped phosphors - a review, Mat. Sci. Res. India. 15 (2018) 252–255.
[11] Y. Zorenko, V. Gorbenko, V. Savchyn, T. Zorenko, T. Martin, P.-A. Douissard, M. Nikl, J.A. Mares, Luminescent properties and energy transfer processes in Ce–Tb doped single crystalline film screens of Lu-based silicate, perovskite and garnet compounds, Radiat. Meas. 56 (2013) 415–419.
[12] J. Langley, M. Litz, J. Russo, W. Ray, Design of Alpha-Voltaic Power Source Using Americium-241 ($^{241}Am$) and Diamond with a Power Density of 10 mW/cm$^3$, ARL-TR, 2017, p. 8189.
[13] E. Sheshin, A. Kolodyazhnyj, N. Chadaev, A. Getman, M. Danilkin, D. Ozol, Prototype of cathodoluminescent lamp for general lighting using carbon fiber field emission cathode, J. Vac. Sci. Technol. B 37 (2019), 031213– 031219.
[14] M. Korjik, K.-T. Brinkmann, G. Dosovitskiy, V. Dormenev, A. Fedorov, D. Kozlov, V. Mechinsky, H.-G. Zaunick, Compact and effective detector of the fast neutrons on a base of Ce-doped $Gd_3Al_2Ga_3O_{12}$ scintillation crystal, IEEE Trans. Nucl. Sci. 66 (2018) 536–540.
[15] G. Dosovitskiy, P. Karpyuk, E. Gordienko, D. Kuznetsova, E. Vashchenkova, P. Volkov, V. Retivov, V. Dormenev, K.-T. Brinkman, H.-G. Zaunick, V. Mechinsky, A. Fedorov, I. Slusar, A. Dosovitsky, M. Korzhik, Neutron detection by Gd-loaded garnet ceramic scintillators, Radiat. Meas. 126 (2019) 106133–106137.
[16] K. Kamada, S. Kurosawa, P. Prusa, M. Nikl, V. Kochurikhin, T. Endo, K. Tsutumi, H. Sato, Y. Yokota, K. Sugiyama, A. Yoshikawa, Cz grown 2-in. size Ce: $Gd_3(Al,Ga)_5O_{12}$ single crystal; relationship between Al, Ga site occupancy and scintillation properties, Opt. Mater. 36 (2014) 1942–1945.
[17] C. Warut, Luminescence and Scintillation Properties of Mg2 +Codoped Lu0.6Gd2.4Al2Ga3O12:Ce Single Crystal, Presented at SCINT2019, 29 September – 4 October, 2019.
[18] C. Warut, Scintillation Characteristics of Mg2 +Codoped Y0.8Gd2.2Al2Ga3O12:Ce Single Crystal, Presented at SCINT2019, 29 September – 4 October, 2019.
[19] A. Potdevin, G. Chadeyron, D. Boyer, R. Mahiou, Optical properties upon vacuum ultraviolet excitation of sol-gel based $Y_3Al_5O_{12}:Tb^{3+}$, $Ce^{3+}$ powders, J. Appl. Phys. 102 (2007), 073536–073543.
[20] T. Yanagida, H. Takahashi, T. Ito, D. Kasama, T. Enoto, M. Sato, S. Hirakuri, M. Kokubun, K. Makishima, T. Yanagitani, H. Yagi, T. Shigeta, T. Ito, Evaluation of properties of YAG (Ce) ceramic scintillators, IEEE Trans. Nucl. Sci. 52 (2005) 1836–1941.
[21] E. Gordienko, A. Fedorov, E. Radiuk, V. Mechinsky, G. Dosovitskiy, E. Vashchenkova, D. Kuznetsova, V. Retivov, A. Dosovitskiy, M. Korjik, R. Sandu, Synthesis of crystalline Ce-activated garnet phosphor powders and technique to characterize their scintillation light yield, Opt. Mater. 78 (2018) 312–318.
[22] P. Lecoq, A. Gektin, M. Korzhik, Inorganic Scintillators for Detector Systems: Physical Principles and Crystal Engineering, second ed., Springer International Publishing, 2017, p. 408.
[23] A. Nakatsuka, A. Yoshiasa, T. Yamanaka, Cation distribution and crystal chemistry of $Y_3Al_{5-x}Ga_xO_{12}$ ($0 \leq x \leq 5$), Acta Crystallogr. B. 55 (1999) 266–272.
[24] A. Sackville Hamilton, G. Lampronti, S. Rowley, S. Dutton, Enhancement of the magnetocaloric effect driven by changes in the crystal structure of Al-doped GGG, $Gd_3Ga_{5-x}Al_xO_{12}$($0 \leq x \leq 5$), J. Phys. Condens. Matter 26 (2014) 116001–116008.
[25] K. Mishra, S. Singh, A. Singh, M. Rai, B. Gupta, S. Rai, New perspective in garnet phosphor: low temperature synthesis, nanostructures, and observation of multimodal luminescence, Inorg. Chem. 53 (2014) 9561–9569.
[26] P. Dorenbos, Exchange and crystal field effects on the $4f^{n-1}5d$ levels of $Tb^{3+}$, J. Phys. Condens. Matter 15 (2003) 6249–6268.
[27] K. Momma, F. Izumi, VESTA 3 for three-dimensional visualization of crystal, volumetric and morphology data, J. Appl. Crystallogr. 44 (2011) 1272–1276.
[28] X. Xu, J. Wang, J.-P. Lv, Y. Deng, Simultaneous analysis of three-dimensional percolation models, Front. Physiol. 9 (2014) 113–119.
[29] U. Gossele, M. Hauser, U. Klein, R. Frey, Diffusion and long-range energy transfer, Chem. Phys. Lett. 34 (1975) 519–522.
[30] R.T. Wegh, A. Meijerink, R.-J. Lamminmaki, J. Holsa, Extending dieke's diagram, J. Lumin. 87–89 (2000) 1002–1004.
[31] S. Nargelas, M. Korjik, M. Vengris, G. Tamulaitis, Study of electronic excitation relaxation at cerium ions in $Gd_3Al_2Ga_3O_{12}$ matrix using multipulse transient absorption technique, J. Appl. Phys. 128 (10) (2020) 103104.